Materials Today Bio 15 (2022) 100324

Contents lists available at ScienceDirect

Materials Today Bio

journal homepage: www.journals.elsevier.com/materials-today-bio

Development of a three-dimensional blood-brain barrier network with opening capillary structures for drug transport screening assays

Marie Piantino [a], Dong-Hee Kang [a], Tomomi Furihata [b], Noriyuki Nakatani [c], Kimiko Kitamura [d], Yukari Shigemoto-Mogami [d], Kaoru Sato [d], Michiya Matsusaki [a,*]

[a] Department of Applied Chemistry, Graduate School of Engineering, Osaka University, Suita, Osaka, Japan
[b] School of Pharmacy, Tokyo University of Pharmacy and Life Sciences, Hachioji, Tokyo, Japan
[c] SCREEN Holdings Co.,Ltd. Development Section 2, R&D Department 1, Furukawa-cho, Hazukashi, Fushimi-ku, Kyoto, Japan
[d] Division of Pharmacology, Laboratory of Neuropharmacology, National Institute of Health Sciences (NIHS), Kawasaki, Kanagawa, Japan

ARTICLE INFO

Keywords:
Blood-brain barrier
In vitro model
Permeability
transferrinReceptor
Drug screening

ABSTRACT

The blood-brain barrier (BBB), a selective barrier regulating the active and passive transport of solutes in the extracellular fluid of the central nervous system, prevents the delivery of therapeutics for brain disorders. The BBB is composed of brain microvascular endothelial cells (BMEC), pericytes and astrocytes. Current *in vitro* BBB models cannot reproduce the human structural complexity of the brain microvasculature, and thus their functions are not enough for drug assessments. In this study, we developed a 3D self-assembled microvascular network formed by BMEC covered by pericytes and astrocyte end feet. It exhibited perfusable microvasculature due to the presence of capillary opening ends on the bottom of the hydrogel. It also demonstrated size-selective permeation of different molecular weights of fluorescent-labeled dextran, as similarly reported for *in vivo* rodent brain, suggesting the same permeability with actual *in vivo* brain. The activity of *P*-glycoprotein efflux pump was confirmed using the substrate Rhodamine 123. Finally, the functionality of the receptor-mediated transcytosis, one of the main routes for drug delivery of large molecules into the brain, could be validated using transferrin receptor (TfR) with confocal imaging, competition assays and permeability assays. Efficient permeability coefficient (P_e) value of transportable anti-TfR antibody (MEM-189) was seven-fold higher than those of isotype antibody (IgG1) and low transportable anti-TfR antibody (13E4), suggesting a higher TfR transport function than previous reports. The BBB model with capillary openings could thus be a valuable tool for the screening of therapeutics that can be transported across the BBB, including those using TfR-mediated transport.

MP and DK carried out the experiments. MP and DK wrote and edited the manuscript. MP, DK, TF, YSM, KK, KS, MM contributed to the design and implementation of the research and to the analysis of the results. All authors have seen and approved the final manuscript.

1. Introduction

The blood-brain barrier (BBB) represents a physical and metabolic barrier that separates the periphery from the central nervous system (CNS). The BBB comprises brain microvascular endothelial cells (BMEC) unsheathed by pericytes and astrocytes [1]. The maintenance of brain homeostasis is ensured by the presence of adherens and tight junctions, efflux systems and specific transporters expressed by BMEC. By strictly regulating the passage of solutes, the BBB also represents a major hurdle for the delivery of many drugs into the extracellular fluid of the CNS. This low penetration of drugs across the BBB limits the development of successful drugs for treating CNS-related diseases [2]. The receptor-mediated transcytosis (RMT) has attracted interest for pharmaceutical companies since it can improve transport efficiency of large molecules, like antibody-drug conjugates, in a non-invasive manner. The RMT is indeed naturally present at the brain endothelium for enabling the delivery of macromolecules necessary for the maintenance of brain function [3,4]. Antibodies or peptide ligands which bind RMT receptors can be grafted on drug delivery systems (DDS) for enabling their brain accumulation [5–8]. The properties of these DDS (i.e. affinity, specificity, valency) need however to be optimized to generate therapeutics with high transportability across the BBB. A fully human BBB model would be helpful to study the mechanisms of drug transportation and screen them

* Corresponding author.
E-mail address: m-matsus@chem.eng.osaka-u.ac.jp (M. Matsusaki).

https://doi.org/10.1016/j.mtbio.2022.100324
Received 28 April 2022; Received in revised form 9 June 2022; Accepted 9 June 2022
Available online 15 June 2022

based on their permeation efficiency into the brain.

Several *in vitro* BBB models have been implemented to optimize the design of new therapies and drug delivery systems. For several decades, transwell assays have been extensively used to predict drug permeability by co-culturing a monolayer of BMEC with pericytes and/or astrocytes. Each cell type can be physically separated by attaching them on both sides of the transwell or on the bottom of the well plate [9]. Although this system represents a cost-effective and reproducible method, it fails to accurately mimic some important BBB features and extracellular matrix (ECM) microenvironment. The two-dimensional configuration and the presence of artificial polyester membrane reduce the possibility of the three cell types of the BBB to communicate directly and make physical contact with each other [10,11]. The lack of exposure of endothelial cells to the physiological mechanical forces such as shear stress also prevent the induction of a BBB phenotype in BMEC [12]. Alternatively, microfluidic platforms have recently emerged to address these issues by offering a closer representation of the *in vivo* microenvironment. These "organ-on-chip" BBB models can reproduce a 3D multicellular configuration by co-culture of several types of BBB cells, physiochemical microenvironment, vascular perfusion under physiological shear stress [13]. For example, systems of perfused vessels in co-culture with supporting cells were engineered [14,15]. However, no direct cell-cell contact was possible between the endothelial cells and the supporting cells since they were physically separated by an acellular collagen type I gel or polycarbonate membrane. It is however known that a direct contact between vascular network and astrocytes is important to achieve a significant reduction in paracellular transport of models compounds as compared monoculture and indirect coculture [16–18]. Additionally, the assembly of microfluidic models is difficult and expensive due to the multi-step preparation and specific equipment required [14,19]. Furthermore, some of these models have a large vessel diameter (~600–800 μm) [14,20], which is much higher than the actual *in vivo* dimensions of the human BBB vasculature, composed of arterioles and venules (10–90 μm diameter) and capillaries (7–10 μm diameter) [21]. As these models cannot effectively recapitulate BBB microvasculature morphology, it may lead to an inaccurate reproduction of the blood flow and transport exchange events occurring in brain capillaries. Although this diameter could be greatly reduced below 30 μm of outer diameter in self-organization models [16,19,22], the "brain" side remains not easily accessible for the sample collection and in-depth composition analysis after transport assays.

The validation of a BBB model usually relies on the assessment of barrier integrity and functionality of specific transport systems. It can respectively be checked by measuring the permeability of the dextran or specific substrates. The size-permeability of different molecular weight of dextran is often investigated in most BBB models to demonstrate the low paracellular transport [13,15,19]. Only few studies however demonstrate the functionality of specific transporters such as the transferrin receptor (TfR) [14,23], known to use the RMT pathway. For example, Wevers et al. investigated the functionality of the TfR by comparing the transcytosis ability of the anti-TfR antibody MEM-189 and control antibody IgG1 [14], with only a two-fold difference was observed. The functionality of the TfR in this model may be not sufficient to distinguish "hit" compounds from other candidates when performing high-throughput screening by transport assays. Therefore, a 3D BBB model displaying higher discrimination of candidate molecules based on their TfR-mediated transport efficiency is expected to improve the sensitivity of the drug screening assays. To perform permeability assays, dextran or other tested compound require the capillaries to have an open end to perfuse molecules inside the capillary lumen. These techniques cannot however be performed in our previously reported 3D self-organized BBB capillary network model due to the absence of a perfusable connection between the outside and the capillary lumen [24,25]. Controlling the capillary organization and opening in our BBB model, as originally reported in 3D blood-/lymph-capillary networks [26], would thus be beneficial for drug transport assays.

In this study, we report the establishment of a 3D self-organized *in vitro* model of the brain microvasculature with perfusable opening structures. This model would not require any special equipment, and would thus be easier and faster to set up than current microfluidic platforms for high-throughput screening. This fully human 3D BBB model recapitulates direct cell-cell interactions between BMEC, astrocytes and pericytes. This model also demonstrates sufficiently low paracellular permeability to enable a size-selective transport of different molecular weight of dextran. The activity of the *P*-gp efflux pump was then validated using the specific substrate Rhodamine 123 which showed a preferential transport from the "brain" side to the "blood" side. Finally, the functionality of specific transport systems, such as the transferrin receptor (TfR), was confirmed by competition assays using its native ligand, transferrin, and permeability assays using TfR-targeted antibodies. Permeability coefficient (P_e) value of transportable TfR antibody (MEM-189) was 7-fold higher than the P_e value of isotype antibody (IgG1) and low transportable antibody (13E4), suggesting a higher functional and efficient TfR-mediated transport as compared to the other previous reports [14]. By mimicking several features of the native BBB in a user-friendly manner, our model shows potential to be used as a platform for screening of CNS drugs transported across the BBB.

2. Materials and methods

2.1. Cell maintenance

The three cell lines used in this study have been developed and characterized in previous studies: human brain microvascular endothelial cells/conditionally immortalized clone 18 (HBEC) [27], human astrocyte/conditionally immortalized clone 35 (HA) [28], and human brain pericyte/conditionally immortalized clone 37 (HP) [29] were kindly provided by Prof. Furihata from the School of Pharmacy, Tokyo University of Pharmacy and Life Sciences (Hachioji, Tokyo, Japan). All cells were cultured on 100 mm diameter collagen type I coated dishes (Ref. 4020–010, Iwaki, Shizuoka, Japan) and incubated at 33 °C, 5% CO_2. All culture media were supplemented with 4 μg/mL Blasticidin S HCl (Ref. R21001, Invitrogen, Waltham, USA) to maintain selective pressure during routine culture. HBEC were cultured in Vasculife (Ref. LEC-LL0005, VEGF-Mv, LifeLine, Frederick, USA) supplemented with 0.5 mL rh FGF-b, 0.5 mL ascorbic acid, 0.5 mL hydrocortisone hemisuccinate, 25 mL l-glutamine, 0.5 mL rh IGF-1, 0.5 mL rh EGF, 0.5 mL rh VEGF, 0.5 mL heparin sulfate, 25 mL fetal bovine serum (FBS) (kit, LifeFactor VEGF-Mv, LifeLine, Frederick, USA), 25 mL supplementary FBS (Gibco ThermoFisher, Waltham, USA), and 1% penicillin-streptomycin (P/S, 10,000 U.mL-1 - 10,000 μg.mL-1, Nacalai tesque, Kyoto, Japan). HA were cultured in Dulbecco's Modified Eagle Medium (DMEM, Ref. 08458–16, Nacalai tesque, Kyoto, Japan), complemented with 10% FBS, 1% P/S, 5 mL of N_2 supplement x100 (Ref. 17, 502,048, Gibco ThermoFisher, Waltham, USA). HP were cultured in Pericyte Medium (Ref. 1201, ScienCell Research Laboratories, Carlsbad, USA), supplemented by 1% Pericyte Growth Supplement 100x, 10% FBS, and 1% P/S. HA and HP were pre-differentiated at 37 °C during 3 days prior to their use for the fabrication of the 3D model BBB model.

2.2. Fabrication of 3D BBB with open structures

The detailed method of preparation of the 3D BBB network with open structures is summarized in Figure S1. One the first day of preparation, a solution of 10%wt gelatin was prepared using gelatin powder (Ref G1890, Sigma Aldrich, St. Louis, MO, USA) dissolved in PBS. This solution was first placed in warm water bath to make it completely dissolved. 450 μL of 10%wt gelatin solution was dispensed on a 24-well plate (Ref. 3820–024, Iwaki, Shizuoka, Japan). The 24-well culture inserts with 0.4 μm pore size (Ref. 3470, Costar, NY, USA) were placed on the gelatin solution by taking precautions to avoid bubbles formation below the insert. The 24-well plate was then incubated at 4 °C for 20 min to

enable the gelation of the gelatin solution. After complete gelation, the inserts were taken out from the gelatin mold and the culture insert membranes was removed. The insert without membranes were plasma-treated with a small plasma device (Ref. PM100, Yamato Scientific Co, Ltd, Tokyo, Japan) with 40 sccm, 100 W for 1 min to make them hydrophilic. The plasma-treated inserts were placed back onto the gelatin mold in the 24-well plate. The HBEC, HA and HP were harvested with a Trypsin/EDTA solution composed of 0.25% trypsin (Ref. 209–19182, Fujifilm Wako, Osaka, Japan) with 0.02% EDTA (Ref. E6758-500G, Sigma Aldrich, St. Louis, MO, USA) and centrifuged at 130 g for 3 min at room temperature. The cell pellet was resuspended in non-complemented DMEM and cell count was performed with the Countess™ 3 Automated Cell Counter (ThermoFisher, Waltham, USA). For the preparation of each 3D BBB gel, 2 mg of fibrinogen (Ref. F8630-5G, Sigma Aldrich, St. Louis, MO, USA) were dispersed in 40 μL of non-complemented DMEM in a Eppendorf tube, while 4×10^5 HA, 2×10^5 HBEC and 2×10^5 HP, and 0.2 U thrombin (Ref. T4648-10kU, Sigma Aldrich, St. Louis, MO, USA) were dispersed in 20 μL of non-complemented DMEM in another Eppendorf tube. The other BBB configurations were prepared in a similar manner but by omitting HP, HA and/or HBEC inside the fibrin gel when necessary. Both solutions were quickly mixed before depositing in cell culture inserts and incubated for 20 min at room temperature for fibrinogen gelation. The fibrins gels were then incubated an additional 40 min at 37 °C, 5% CO_2 to dissolve the gelatin gels. After complete dissolution of the gelatin gels, 500 μL of PBS was added into the bottom of the 24-well plates. The fibrin gels were placed in a new well with 2.5 mL of triple media composed of Vasculife medium, Pericyte medium, and DMEM/N_2 medium (1:1:1; v:v:v), all without Blasticidin, and incubated at 37 °C, 5% CO_2 overnight.

On the next day, the insert with fibrin gel was placed upside down in a 6-well plate (Ref. 3810–006, Iwaki, Shizuoka, Japan) filled with 10 mL of triple media. HBEC was harvested for a second seeding on the fibrin gel, with 2×10^5 HBEC resuspended in 60 μL of triple media on top of each fibrin gel. The gels were incubated at 37 °C, 5% CO_2 to enable the adhesion of HBEC onto the fibrin gel. After 6 h incubation, the inserts were placed on top of 6 well culture plates thanks to a specifically designed 24- to 6-well plate adaptor. 4 mL of triple media were additionally added and incubated at 37 °C & 5% CO_2. Half of the media (7 mL of total 14 mL) was changed every 3–4 days before the subsequent experiments performed after 7 days of culture.

2.3. Immunofluorescence staining

After 7 days culture, the 3D BBB models were rinsed three times in PBS then fixed in 4% paraformaldehyde (PFA, Fujifilm Wako, Osaka, Japan) at room temperature (RT) for 15 min. Permeabilization was carried out using 0.2% Triton X-100 diluted in PBS for 15 min (Sigma-Aldrich, St. Louis, MO, USA). After PBS rinsing, blocking was performed for 1 h at RT with 1% bovine serum albumin (BSA, Ref. A3294-50G, Sigma-Aldrich, St. Louis, MO, USA) in PBS. The samples were incubated with primary antibodies overnight at 4 °C: mouse anti-human CD31 antibody (Ref. NCL-CD31-1A10, Leica, Wetzlar, Germany), mouse anti-human ZO-1 antibody (Ref. ZO1-1A12, Invitrogen, Waltham, MA, USA, or mouse anti-human Claudin-5 antibody (Ref. 35–2500, Thermo Fisher Scientific, Waltham, MA, USA) diluted at 1/100 in 1% BSA in PBS. After PBS rinsing, samples were incubated for 2 h at room temperature in the dark with secondary antibody goat anti-mouse conjugated with Alexa Fluor 647 (Ref. A21235, Thermo Fisher Scientific, Waltham, MA, USA) diluted at 1/100 in 1% BSA in PBS. Actin filaments were stained with fluorescein isothiocyanate (FITC)-labeled phalloidin (Ref. ab235137, Abcam, Cambridge, UK). The nuclei were counterstained with Hoechst33342 (Ref. H3570, Thermo Fisher Scientific, Waltham, MA, USA). After washing three times with PBS, the samples were observed with confocal laser scanning microscope FluoView FV3000 (Olympus, Tokyo, Japan) using × 10 or × 40 magnification.

2.4. Calculation of $CD31^+$ surface area in the 3D BBB models

The whole insert was imaged by taking large scale pictures of the 3D BBB models stained for CD31 using confocal laser scanning microscope FluoView FV3000 (Olympus, Tokyo, Japan) using × 10 magnification. Three sections of the 3D BBB gel (bottom, middle and top of the fibrin gel) were separately imaged for three BBB gels issued from three independent experiments. The observation settings were kept the same for imaging the 3D BBB gels, such as the step size, the thickness of each observed section, the exposition time and excitation power. The $CD31^+$ surface area was automatically generated by IMARIS software for the three sections of the 3D BBB gels (Oxford Instruments, Abingdon, UK). The total $CD31^+$ surface area for each was obtained by summing the $CD31^+$ surface area of the three sections of the gel (bottom, middle and top of the fibrin gel).

2.5. Leakage assay with fluorescein isothiocyanate labeled dextran

The perfusability of the open structures was assessed by adding a solution of 1 mg/mL FITC-dextran MW 2000 kDa (Ref. FD2000S, Sigma Aldrich, St. Louis, MO, USA) diluted in PBS in the bottom side of the insert. After 1 h incubation at room temperature, observation by confocal microscopy was performed by confocal laser scanning microscope FluoView FV3000 (Olympus, Tokyo, Japan) using x60 magnification. This experiment was conducted using fixed samples.

2.6. Imaging with optical coherence tomography (OCT)

The OCT system Cell^{3}iMager Estier (SCREEN Holdings Co, Ltd, Kyoto, Japan) was used to confirm the microvasculature of the fabricated 3D BBB model in a label-free manner [30]. After 7 days culture, the 3D BBB model was fixed by the same method mentioned in section 2.3. After the sample loading, the OCT imaging was performed using magnification 10x, with a scan size of 500 μm × 500 μm, a pitch of 2 μm and layer pitch of 20 μm.The movie was created by combining the slice images from OCT imaging.

2.7. Evaluation of the transepithelial electrical resistance

The transepithelial electrical resistance (TEER) was measured for the fibrin gel without BBB cells and for 3D BBB model with open structures after 7 days culture. The TEER was measured in PBS at RT using a Millicell® ERS-2 Volt-Ohm Meter (Millipore, Bedford, MA, USA) equipped with a STX01 chopstick electrode (Millipore, Bedford, MA, USA). The TEER value was calculated from the following equation (1) [31]:

$$TEER = (R_{BBB} - R_{only\ gel}) \times A \quad (1)$$

where $R_{only\ gel}$ is the resistance of the fibrin gel without BBB cells; R_{BBB} is the resistance of the fibrin gel seeded with BBB cells, and A is the average value of $CD31^+$ surface area of three 3D BBB gels calculated by IMARIS software.

2.8. Histology

After 7 days culture, the 3D BBB model with open structures were rinsed with PBS and fixed with 4% PFA at RT for 15 min. The samples were sent to the Applied Medical Research Company for paraffin wax embedding, sections mounting, CD31 and hematoxylin and eosin (H&E) staining. The sections were then observed using the FL Evos Auto microscope (Thermo Fisher, Waltham, USA).

2.9. Visualization of TfR-mediated endocytosis

The HBEC monolayer was co-incubated with 10 μg/mL Alexa Fluor 488-transferrin (AF 488-Tf, (Ref. 009-540-050, Jackson

ImmunoResearch, West Grove, PA, USA) and 10 μg/mL Alexa Fluor 647-MEM-189 (AF 647 MEM-189, Ref. NB500-493AF647, NovusBio, Centennial, USA) for 1 h at 37 °C, 5% CO_2. The samples were then fixed with 4% PFA and washed three times with PBS prior to the confocal observation. Images were then taken with a confocal laser scanning microscope AX (Nikon, Tokyo, Japan).

2.10. Permeability assays

One day prior to the permeability assays, the wells of 24-well plate were pre-incubated with 1 mL of 1% BSA (Ref. A3294, Sigma Aldrich, St. Louis, MO, USA) in PBS overnight at 37 °C, 5% CO_2 to prevent unspecific adsorption of the tested molecules on the walls of the plate. All the permeability assays were performed on day 7 and day 8 of culture of the 3D BBB models at 37 °C, 5% CO_2 in triple media, using 1000 μL of triple media in the bottom side and 200 μL in the top side of the inserts.

For the assessment of paracellular transport, 4 kDa (Ref. T1037, Sigma Aldrich, St. Louis, MO, USA), 20 kDa (Ref. 73,766, Sigma Aldrich, St. Louis, MO, USA) and 70 kDa (Ref. T1162, Sigma Aldrich, St. Louis, MO, USA) of tetramethylrhodamine (TRITC)-labeled dextran at a final concentration of 1 mg/mL or 10 μM Lucifer Yellow (CH, dilithium salt) (Ref. L0259, Sigma-Aldrich, St. Louis, MO, USA) were added to the bottom side before beginning the assay. 10 μL of the culture media was collected in the top side of the insert at t = 1 h, 10 h, 24 h for the analysis.

For the evaluation of the functionality of *P*-glycoprotein (*P*-gp), the transport of Rhodamine 123 (Ref. R302, Thermo Fisher Scientific, Waltham, MA, USA) was measured for both the apical-to-basolateral side or basolateral-to-apical side. For that, 10 μM Rhodamine 123 dissolved in triple media was added in the bottom side (apical-to-basolateral transport) or top side (basolateral-to-apical transport) of the inserts containing the 3D BBB gels. Triple media was added in the top side (apical-to-basolateral transport) or bottom side (basolateral-to-apical transport) without the tested molecule. 10 μL of the culture media was collected in the top side (apical-to-basolateral transport) or the bottom side (basolateral-to-apical transport) of the insert at t = 1 h, 5 h, 10 h, 24 h for the analysis.

For the receptor-mediated transcytosis assay, 10 μg/mL Alexa Fluor 647-MEM-189 (AF 647-MEM-189, Ref. NB500-493AF647, NovusBio, Centennial, USA), Alexa Fluor 647-13E4 (AF 647-13E4, Ref. NB100-73092, NovusBio, Centennial, USA) or Alexa Fluor 647-immunoglobulin G1 (AF 647-IgG1, Ref. NBP1-97005AF647, NovusBio, Centennial, USA) was added in the bottom side of the insert during 24 h 10 μL of the culture media was collected in the top side of the insert at t = 1 h, 5 h, 10 h, 24 h for the analysis.

For the competition binding assays to the TfR, Alexa Fluor 488-transferrin (AF 488-Tf, Ref. 009-540-050, Jackson ImmunoResearch, West Grove, PA, USA) at a final concentration of 10 μg/mL was co-incubated with various concentrations of unlabeled transferrin (Tf, Ref. 009-000-050, Jackson ImmunoResearch, West Grove, PA, USA) at a final concentration of 0, 10 or 20 μg/mL in the bottom side of the insert. 10 μL of the culture media was collected in the top side of the insert at t = 1 h, 5 h, 10 h for the analysis.

The fluorescent intensity of the tested molecules was evaluated using Nanodrop™ fluorospectrometer (N3300, Thermo Fisher Scientific, Waltham, MA, USA) from which was deduced the amount of transported compound across the fibrin gel. The cumulative amount transported across the membrane was plotted against time, and the slopes of the linear regions were used to calculate the permeability coefficients, as previously reported [32,33]:

The apparent permeability coefficient (P_{app}) was calculated using the following equation (2):

$$P_{app} = (dQ/dt)/ (C_0 \times A) \quad (2)$$

where dQ/dt is the transport rate, defined as the slope obtained from linear regression of the transported amount, C_0 is the initial concentration on the donor side and A is the average value of $CD31^+$ surface area of the 3D BBB gel calculated by IMARIS software.

The effective permeability coefficient (P_e) of the 3D BBB gel was calculated using the following equation (3):

$$PS = (dQ/dt)/ (D_0 \times A \quad (3)$$

With PS, dQ/dt, and D_0 being respectively the permeability surface area product, the slope of the linear region of a plot of the amount of permeant in the receiver chamber over time, and the initial concentration of the tested molecule on the donor side.

$$1/PS_{total} = 1/PS_e + 1/PS_{only\ gel} \quad (4)$$

$$P_e = PS_e/A \quad (5)$$

with PS_{total} and $PS_{only\ gel}$ being respectively the permeability surface area product corresponding to the 3D fibrin gel seeded with and without the three types of BBB cells and PS_e is the surface area product value for the 3D BBB cells. A is the average value of $CD31^+$ surface area of the 3D BBB gels calculated by IMARIS software.

2.11. Statistical analysis

All values are presented as means ± standard deviation (SD). Statistical analysis of the data was performed with Student's *t*-test or One-way *ANOVA* using EzAnova software (Version 0.985, University of South Carolina, Columbia, SC, USA) when more than two samples were compared with Tukey multiple comparison post-hoc tests. Differences were considered statistically significant when $p < 0.05$.

3. Results and discussion

3.1. Fabrication of a three-dimensional brain microvasculature network model with open structures

A three-dimensional (3D) model of the 3D BBB microvascular network was established as illustrated in Figure S1. Briefly, the HBEC, HA and HP mixture was dispersed in the culture medium containing thrombin. The cell suspension was mixed with fibrinogen and quickly deposited in the 24-well insert before the formation of the fibrin gel. The ratio of each cell type incorporated in the fibrin gel was already established and optimized in a previous report [25]. Based on network appreciation by confocal observations and capillary diameter and length measurements, the best results were obtained for ratios of 1:2:0.5 HBEC:HA:HP. The selected cell ratio was in a similar order of magnitude than those observed *in vivo*, such as 1:5:1 HBEC:HA:HP [34] or 1:0.3 HBEC:HP [35]. The next day, a HBEC monolayer was deposited onto the bottom side of the membrane-free insert of the fibrin gel. The expected mechanism of the formation of the open structures is detailed in Fig. 1. After 7 days culture, the HBEC monolayer and the HBEC inside the fibrin gel fused to generate a vascular network by self-organization with lumen structures, as similarly shown in our previous works [25,36]. Several holes, named open structures, were uniformly distributed in the entire bottom surface of the fibrin gel (Fig. 2A, Figure S2). The confocal xz and yz planes showed a clear organization of the HBEC as capillary-like tubules with open lumen (Fig. 2B, Movie S1, S2). Moreover, the actin and CD31 staining showed the direct cell-cell contact between HBEC, HP and HA (Movie S2). This observation is consistent with previous studies which demonstrated HA and HP were found in the close vicinity of the HBEC network [24,25]. The open structures could be successfully perfused by 2000 kDa dextran (Fig. 2C). Histological sections further confirmed the presence of those open structures and the vascular network inside the fibrin gel with lumen whose diameter varies from 10 to 100 μm (Fig. 2D, E, Figure S3, Movie S3). These values are close to the dimensions of human cerebral capillaries of 7–10 μm and arterioles and

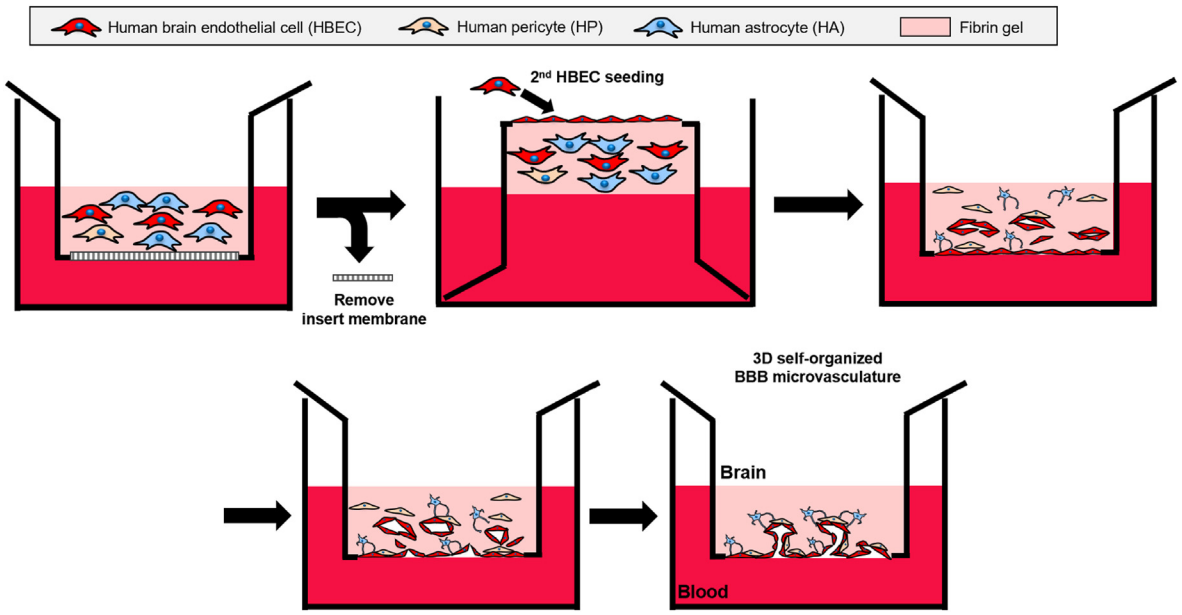

Fig. 1. Schematic illustration of the expected formation of the open structures in 3D BBB model.

venules with a diameter size ranging from 50 to 100 μm [21]. These data suggested the successful formation of open structures composed of BBB microvascular network.

Supplementary data related to this article can be found at https://doi.org/10.1016/j.mtbio.2022.100324.

3.2. Optimization of self-assembled microvasculature with open structures

We next wanted to understand whether there would be one specific cell type which could more contribute for stimulating the formation of the open structures in our model. As seen in Fig. 3A, different combinations of the three BBB cell types were envisaged, with (i) only a monolayer of HBEC on the bottom of the insert ("HBEC mono"), or in combination with (ii) HP ("HBEC mono + HP"), (iii) HA ("HBEC mono + HA"), or (iv) both HP and HA ("HBEC mono + HP + HA"), or (v) HA, HP and HBEC ("HBEC mono + HP + HA + HBEC") inside the fibrin gel. The $CD31^+$ surface area was not significantly changed between the different BBB models, although the highest value was obtained for "HBEC mono + HP + HA + HBEC" condition (Figure S4). Open structures were not formed with "HBEC mono" conditions but were present in "HBEC mono + HP", "HBEC mono + HA", "HBEC mono + HP + HA", and "HBEC mono + HP + HA + HBEC" conditions, with a respective number of open structures of 53 ± 6, 131 ± 8, 223 ± 20 and 301 ± 28 (Fig. 3A). Only a few open structures were observed in "HBEC mono + HP" condition. The addition of HBEC inside the gel enabled the stabilization of a more developed vasculature with more open structures found in "HBEC mono + HP + HA + HBEC" (Fig. 3B and C). Fewer open structures were found in "HBEC mono + HA" condition than with "HBEC mono + HP + HA + HBEC" (Fig. 3C). Open structures were more numerous on the bottom of the gel for "HBEC mono + HA" than for "HBEC mono + HP" condition. These results suggest HA could be more necessary than HP to promote the formation of the open structures in the fibrin gel. This observation is consistent with previous report which also emphasizes the role of astrocytes in the improved morphology of the vascular network [19]. Astrocytes have indeed a major role in the development and maintenance of BBB features in BMEC. They can secrete several growth factors, such as vascular endothelial growth factor (VEGF), basic fibroblast growth factor (bFGF), glial cell line-derived neurotrophic factor (GDNF), or angiopoietin 1 (ANG-1), which can stimulate vasculogenesis, the expression of tight junctions and enzymatic systems and promote the polarization of transporters in HBEC [18,37]. The diameter of these open structures, when present, was in a similar range, independently of the cell combination inside the fibrin gels (Fig. 3C). The formation of open structures is expected to result from the combination of biochemical and physical effects that promotes *in vitro* vascularization in engineered 3D-microenvironments. The HBEC are indeed able to migrate in a 3D environment by attaching to and degrading the surrounding ECM environment. They migrate mainly towards the tissue surface through angiogenic processes under the conditions that large amounts of angiogenic factors (e.g. VEGF) are secreted by neighboring supporting cells [38]. This method enables the 3D arrangement of HBEC that allows their encounter and connection with each other inside the fibrin gel and with those seeded on the bottom of the hydrogel in order to spontaneously form the HBEC capillary network with open structures. Based on the structural evaluation of the vascular network and the highest number of open structures, "HBEC mono + HP + HA + HBEC" was considered as the best combination after 7 days culture and was thus used for the subsequent experiments.

3.3. Evaluation of the barrier function properties

The BBB is characterized by its reduced paracellular transport, with 100% of the large molecules and 98% of small molecules which cannot penetrate the brain [39]. Even the movement of small ions such as Na^+ and Cl^- is also restricted, resulting in a high transendothelial electrical resistance (TEER) that reach more than 1,000 Ω x cm^2 [40,41]. We thus sought to investigate if our model could reproduce this reduced paracellular transport *in vitro*. The TEER value measured in our 3D model was about 560 Ω x cm^2, which is higher than the acellular fibrin gel which has a TEER of about 51 Ω x cm^2 (Figure S5) and the previously reported TEER value of 2D HBEC monolayer of about 20 Ω x cm^2 [42]. Additionally, the paracellular marker Lucifer Yellow showed an apparent permeability coefficient value (P_{app}) and effective permeability coefficient value (P_e) of 8.51 × 10^{-7} cm/s and 4.17 × 10^{-6} cm/s respectively (Fig. 4A and Figure S6). The P_{app} value of Lucifer Yellow is in the same order range (10^{-7} cm/s) than the *in vivo* permeability values measured in pial post-capillary venules in a rodent model, reported to be around 1–2 x 10^{-7} cm/s [43]. Additionally, this P_{app} value is lower than the previously reported values in vascular models using HUVEC or immortalized BMEC [44,45].

The permeability of TRITC-dextran with different molecular weights (4, 20 and 70 kDa) was also evaluated across the 3D BBB model with open structures. As seen in Fig. 4B, the permeability of TRITC-dextran

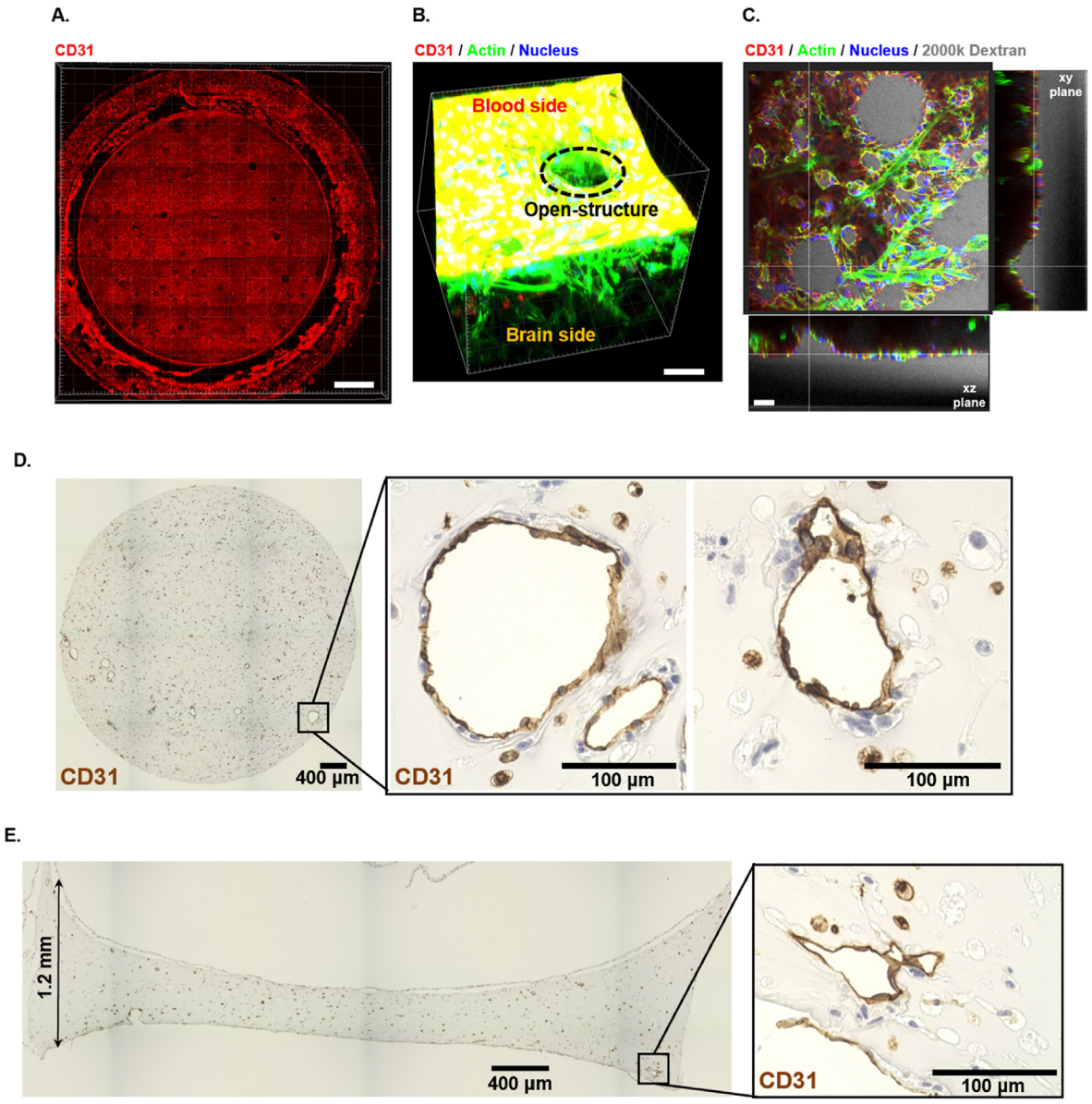

Fig. 2. (A) Confocal image of the bottom side of the whole culture insert after 7 days culture showing the open structures. Scale bar = 1 mm. (B) 3D reconstruction of a confocal z-stack showing the open structures. HBEC were labeled with CD31 (red), all cells were stained for actin filaments (green) and nucleus (blue). Scale bar = 80 µm. (C) Cross-sectional image of the open structure perfused with FITC-labeled dextran (MW 2000 kDa). Scale bar = 50 µm. (D) Histological observations of the bottom side of the insert showing open structures formed by HBEC, stained for CD31 (brown). Hematoxylin was used to stain cell nuclei (purple). (E) Histological observations of a cross-sectioned gel, with lumen surrounded by HBEC stained for CD31 (brown). Hematoxylin was used to stain cell nuclei (purple).

gradually decreased with increased molecular weight, resulting from the different size of tested molecules transported across the 3D BBB model with open structures (Figure S7). The P_{app} value of TRITC-labeled dextran of 4 kDa, 20 kDa, and 70 kDa were respectively 3.63×10^{-7}, 9.22×10^{-8}, 8.84×10^{-8} cm/s (Figure S8). The P_e value of 4 kDa, 20 kDa, and 70 kDa TRITC-labeled dextran were respectively 2.14×10^{-6}, 6.34×10^{-7}, and 4.76×10^{-8} cm/s (Fig. 4B). The P_e values of the dextran correlated with the previously reported *in vivo* rodent brain uptake ($R^2 = 0.973$) (Fig. 4C) [46]. It should also be noted that our model showed a better correlation with *in vivo* values than those previously reported using iPSC-based BBB-Chip model ($R^2 = 0.96$) [13].

The expression of tight junctions (TJs) is known to have an important role in the regulation of the diffusion of molecules across the brain endothelium [47]. Claudin 5 is one of the dominant TJ proteins in the brain endothelium and is thought to play a major role in the macromolecular assembly of the TJs [48]. Zonula occludens-1 (ZO-1) is also involved in the maintenance of the TJs stability and functionality by serving as a linker molecule between the TJ components and the actin cytoskeleton [49–51]. Both ZO-1 and Claudin-5 were expressed by HBEC after 7 days culture both inside and in the bottom of the hydrogel (Fig. 4D). The high expression of the TJs could be partially responsible for the size-selective permeation of dextran and the low transport of the paracellular tracer Lucifer Yellow. Taken together, these results demonstrate that our model could be reliable to predict the brain penetrability of candidate molecules due to the formation and maintenance of a restrictive barrier sufficient for enabling the size-selective transport of molecules.

3.4. Evaluation of efflux pump activity

The presence of specific transport systems on the membranes of BMEC contributes to the regulation of the passage of molecules across the

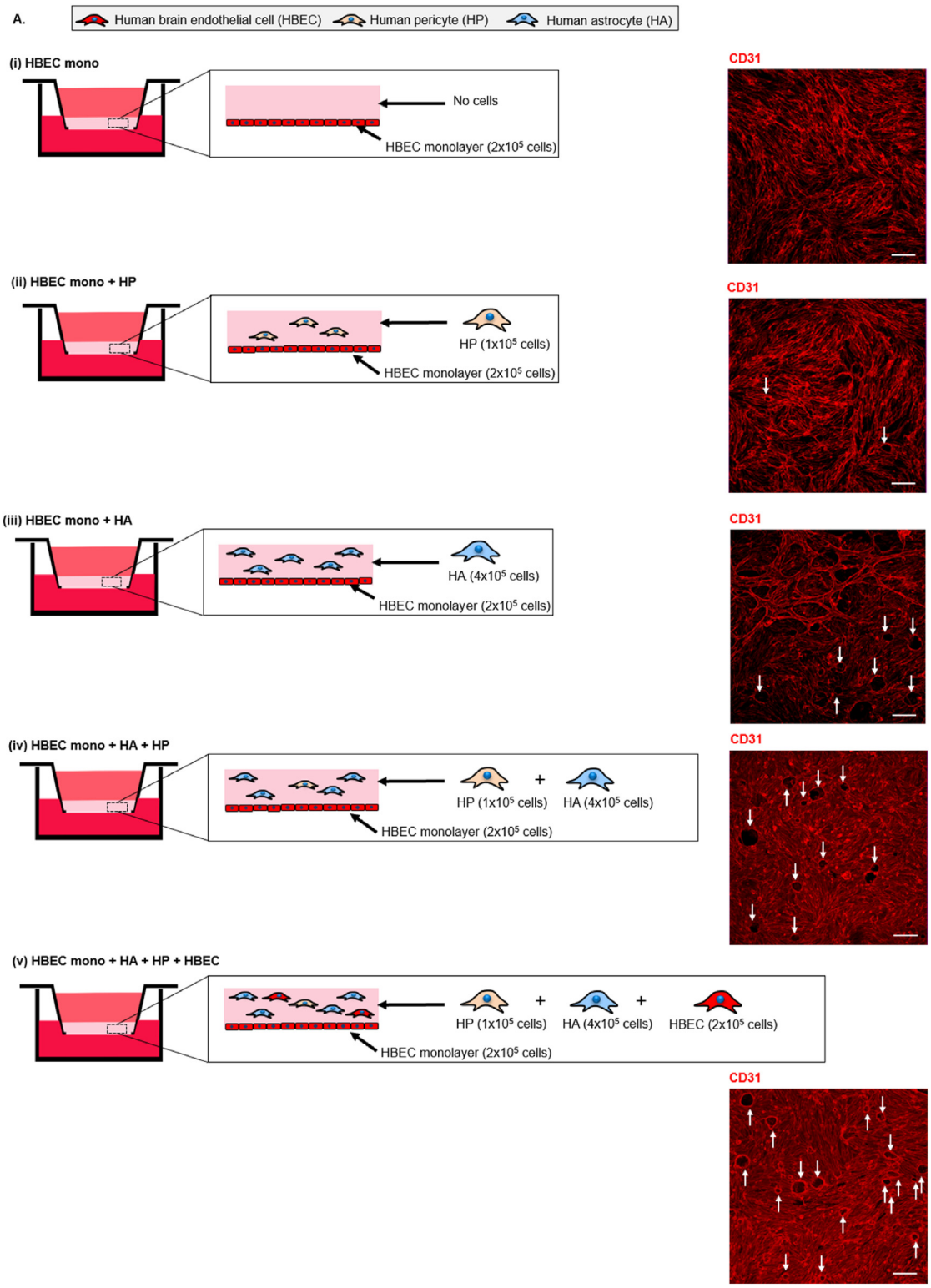

Fig. 3. (A) Comparison of different types of BBB model with the HBEC monolayer seeded on the bottom of the fibrin gel (HBEC mono), with the HBEC monolayer seeded on the bottom of the fibrin gel and only HP (HBEC mono + HP) or only HA (HBEC mono + HA) or both HP and HA inside the fibrin gel (HBEC mono + HA + HP), or with the HBEC monolayer seeded on the bottom of the fibrin gel and HBEC, and HBEC, HP and HA inside the fibrin gel (HBEC mono + HA + HP + HBEC). Confocal images of the bottom side of the culture insert after 7 days culture for the different types of BBB model, HBEC were stained by the endothelial cell marker CD31 (red). White arrows indicate the open structure. Scale bar = 150 μm. (B) Confocal images of the bottom side of the whole culture insert after 7 days culture for the different types of BBB model, HBEC were stained by the endothelial cell marker CD31 (red). Scale bar = 1000 μm. (C) Quantification of number (top) and average diameter (bottom) of open structures at the bottom side of the whole culture insert after 7 days culture for the different types of BBB model (n = 3 gels/condition). The average diameter was determined using 25 open structures per gel were used. Data are presented as means ± S.D. Statistical analysis was performed using one-way *ANOVA* (*$p < 0.05$, n. s. $p \geq 0.05$).

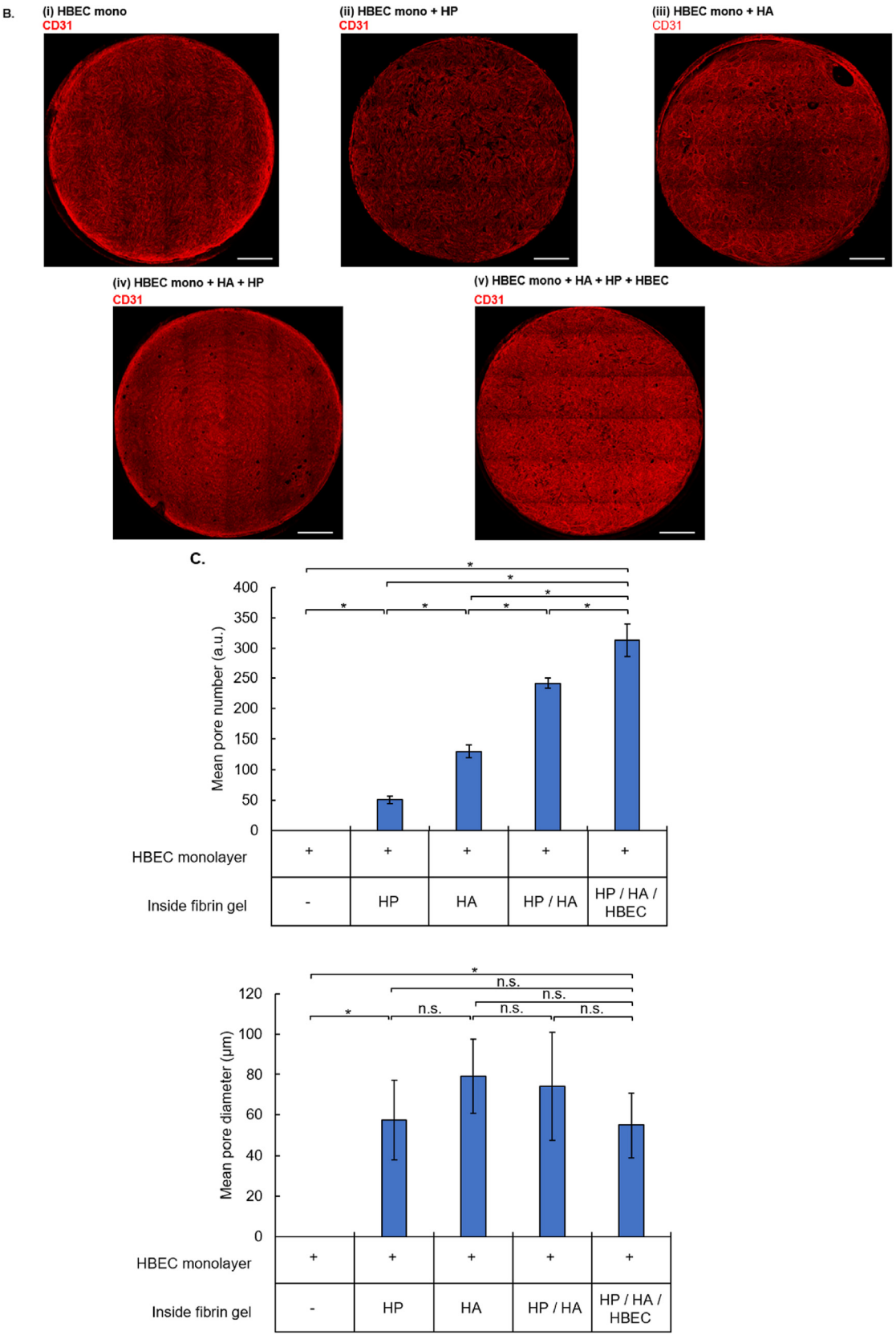

Fig. 3. (*continued*).

BBB, preventing potentially harmful compounds from entering in the brain and effluxing brain metabolic wastes [18]. Efflux transporters localized on the luminal surface of BMEC enable the clearance of potentially harmful xenobiotics from the brain and limit the access of toxic agents to the brain [52]. *P*-glycoprotein (*P*-gp) is one of the most studied efflux pumps responsible for rejection of a wide range of

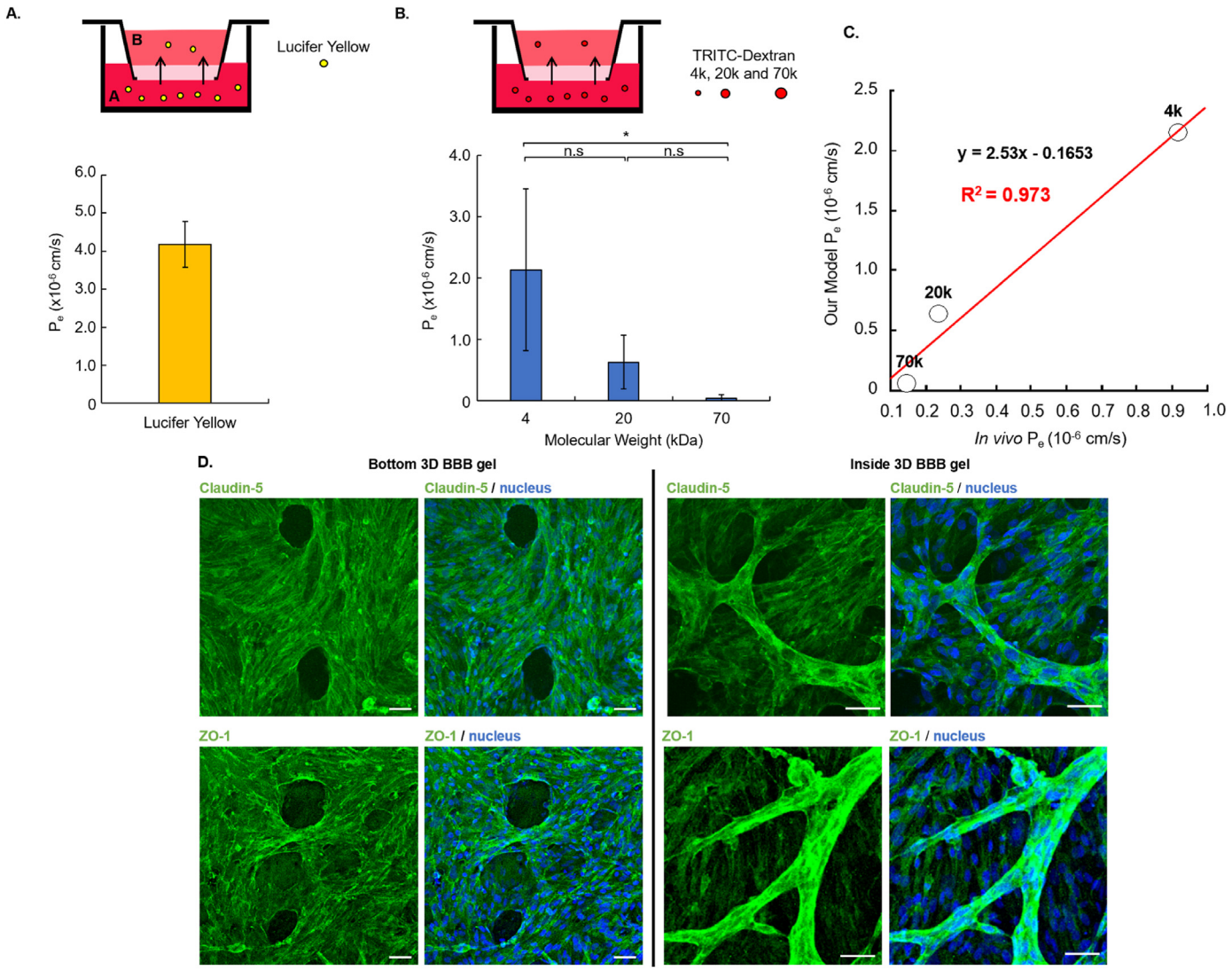

Fig. 4. Characterization of the barrier function properties of 3D BBB model with open structures. (A) Effective permeability coefficient (P_e) of 10 μM Lucifer Yellow after 24 h incubation at 37 °C (n = 3). Data are presented as means ± S.D. (B) P_e values of 1 mg/mL TRITC-dextran with different molecular weights (n = 4). Data are presented as means ± S.D. Statistical analysis was performed using one-way *ANOVA* (*$p < 0.05$, n. s. $p \geq 0.05$). (C) The permeability of dextran molecules across the 3D BBB model with open structures correlated ($R^2 = 0.973$) with previously reported *in vivo* rodent brain uptake (P_e, cm/s). (D) Immunofluorescence staining of the TJs, Claudin-5 (green, top) or ZO-1 (green, bottom) and cell nuclei (blue) in the bottom and inside the 3D BBB model with open structures after 7 days culture. Scale bar = 50 μm.

chemical compounds, including CNS drugs [53]. Although the expression of *P*-gp by HBEC at both gene and protein levels was confirmed in 3D model in a previous study [24], its functionality was yet to be investigated. Since transporter expression is indeed not necessarily correlated with its activity [54], it was primordial to confirm the functionality of the efflux pump in our model. For that, both apical-to-basolateral (A to B) and basolateral-to-apical (B to A) permeability of Rhodamine 123, a specific substrate of *P*-gp [55], was measured. The P_{app} value of Rhodamine 123 from A to B and from B to A was respectively 7.35×10^{-7} and 1.05×10^{-5} cm/s (Figure S9). As seen in Fig. 5A, the P_e value of Rhodamine 123 from A to B compartment and from B to A compartment was respectively 1.95×10^{-6} and 1.91×10^{-5} cm/s. The efflux ratio, defined as $P_{e(B\ to\ A)}/P_{e(A\ to\ B)}$, is about 9.7, demonstrating the high polarization of the *P*-gp, with a higher expression on the apical side, which is similar to *in vivo* situation [56,57].

3.5. Assessment of transferrin receptor-mediated transport

The RMT pathway has been particularly well described for the transferrin receptor (TfR), which mediates the transport of iron-bound transferrin (Tf) [4,58]. TfR has recently attracted increasing attention due to its high expression by both brain BMEC and brain cancer cells, which could be useful for the specific transport of large-sized drugs across the BBB and to the cancer site [59–61].

We first sought to investigate if HBEC were able to mediate the internalization into their cytoplasm of specific substrates of the TfR. The colocalization between Alexa Fluor 488-transferrin (AF 488-Tf), the native ligand of the TfR, and Alexa Fluor 647-MEM-189 (AF 647-MEM-189), a transportable antibody targeting TfR, demonstrated that AF 488-Tf was endocytosed by HBEC through the binding to the TfR (Figure S10). A competition assay was also performed between unlabeled transferrin (Tf) and AF 488-Tf to further confirm the presence of the TfR-mediated transport. For that, different concentration of unlabeled Tf were tried by keeping constant the concentration of AF 488-Tf. As seen in Figure S11A, the permeability of AF 488-Tf tended to decrease when increasing the concentration of unlabeled Tf. The proposed mechanism to explain this phenomenon is illustrated in Figure S11B. AF 488-Tf can be normally transported in the absence of unlabeled Tf. The predominance

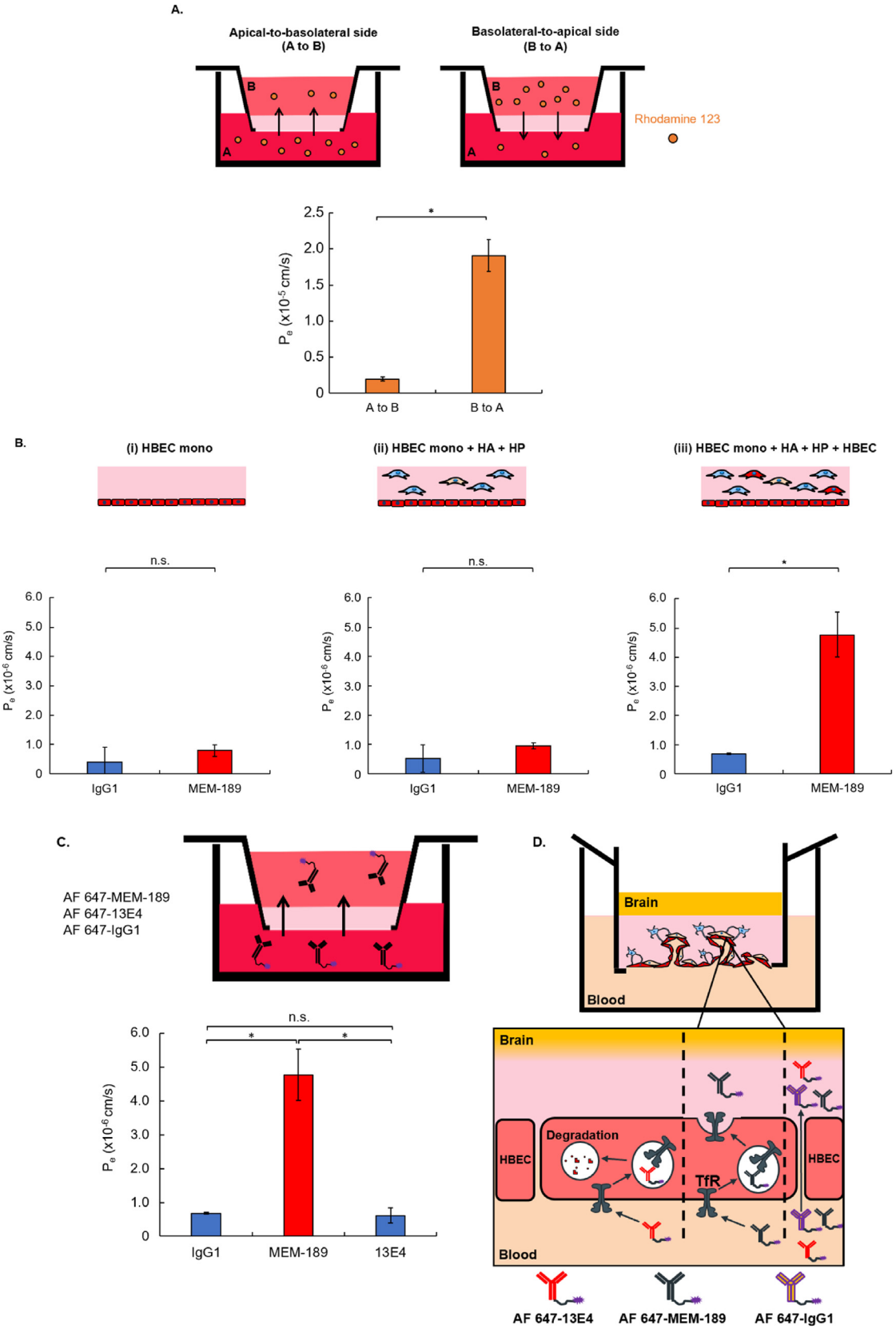

Fig. 5. (A) Comparison of the effective permeability coefficient (P_e) of 10 μM Rhodamine 123 from apical-to-basolateral side (A to B) and basolateral-to-apical side (B to A) after 24 h incubation at 37 °C (n = 3). Data are presented as means ± S.D. Statistical analysis was performed using Student's *t*-test (*$p < 0.05$, n. s. $p \geq 0.05$). (B) P_e values of 10 μg/mL AF 647-MEM-189 or AF 647-IgG1 using different 3D BBB models after 24 h incubation at 37 °C (n = 3). Data are presented as means ± S.D. Statistical analysis was performed using Student's *t*-test (*$p < 0.05$, n. s. $p \geq 0.05$). (C) P_e values of 10 μg/mL AF 647-MEM-189, AF 647-13E4 or AF 647-IgG1 using 3D BBB model with open structures after 24 h incubation at 37 °C (n = 3). Data are presented as means ± S.D. Statistical analysis was performed using one-way *ANOVA* (*$p < 0.05$, n. s. $p \geq 0.05$). (D) Expected mechanism of the permeation of AF 647-MEM-189, AF 647-13E4 or AF 647-IgG1 in the 3D BBB model with open structures.

of unlabeled Tf however resulted in the reduction of the transported amount of AF 488-Tf in the top side of the insert. It could be due to a decrease of the probability for AF 488-Tf to bind the TfR due to the competition with unlabeled Tf for the binding to the TfR. This result showed that the TfR-mediated transport can be modulated in our model when co-incubating molecules competing for the same or overlapping binding sites to the TfR.

We next sought to confirm whether the combination "HBEC mono + HP + HA + HBEC" showed the highest TfR-mediated transport efficiency as compared to "HBEC mono" and "HBEC mono + HP + HA" conditions. For that, the permeability of AF 647-MEM-189 and the mouse Alexa Fluor 647-Immunoglobulin G1 isotype control (AF 647-IgG1), which does not bind any target on human cells, were compared for each model configuration (Fig. 5B, Figure S12). The P_e value of AF 647-MEM-189 was 4.06×10^{-6} cm/s for "HBEC mono + HP + HA + HBEC", which is higher than that of "HBEC mono" and "HBEC mono + HP + HA" conditions, which have a respective P_e value of 7.96×10^{-7} and 9.54×10^{-7} cm/s (Fig. 5B). AF 647-IgG1 showed comparable low permeability for all the configurations, with a respective P_e value of 4.07×10^{-7}, 5.22×10^{-7} and 6.83×10^{-7} cm/s for "HBEC mono" "HBEC mono + HP + HA" and "HBEC mono + HP + HA + HBEC" conditions. Although the number of open structures was the highest in "HBEC mono + HP + HA + HBEC" condition as compared to the "HBEC mono" and "HBEC mono + HP + HA" conditions (Fig. 3C), it did not significantly affect the permeability of AF 647-IgG1, which stayed in the same range of Pe value in the three conditions, suggesting a maintained barrier function and paracellular transport efficiency of the antibodies comparable among the different BBB models. These results suggest "HBEC mono + HP + HA + HBEC" displayed the highest TfR functionality, due to the higher transport of AF 647-MEM-189 as compared to the negative control AF 647-IgG1. The observed differences of permeability between AF 647-IgG1 and AF 647-MEM-189 did not depend on the number of open structures or differences in barrier function, but resulted from the higher TfR-mediated transport in "HBEC mono + HP + HA + HBEC" condition. In order to further characterize the permeation of TfR ligands in the "HBEC mono + HP + HA + HBEC" condition, we next compared the permeability of AF 647-MEM-189 with another human anti-TfR antibody Alexa Fluor 647-labeled 13E4 (AF 647-13E4), reported to have a reduced transportability [23,62]. The P_{app} value of AF 647-MEM-189 was 6.37×10^{-7} cm/s, which is three times higher than that of AF 647-IgG1 and AF 647-13E4, with a respective P_{app} of 2.24×10^{-7} and 2.17×10^{-7} cm/s (Figure S13). A similar trend was found for the P_e values, with 4.77×10^{-6} cm/s for AF 647-MEM-189, which was seven-fold higher than that of AF 647-IgG1 and AF 647-13E4 which are respectively 6.83×10^{-7} and 6.12×10^{-7} cm/s (Fig. 5C). It is worth mentioning that our model displayed a better capacity to discriminate antibodies based on their TfR-mediated permeation than the OrganoPlate©, where only a two-fold difference was observed between the permeability of MEM-189 and IgG1 [14]. The expected mechanism of permeation of the antibodies is detailed in Fig. 5D. 13E4 is reported to have a reduced transportability as a consequence of its high affinity to the TfR. The binding affinity to the TfR has been indeed already reported to determine the transportability of antibodies directed against the TfR, including MEM-189 and 13E4 [62]. Due to its high affinity to the TfR, 13E4 is degraded inside the cells, thus is not transported across the HBEC network in the 3D BBB model. Conversely, since MEM-189 have a moderate affinity to the TfR, it can be efficiently transported by the TfR. Moreover, AF 647-MEM-189, AF 647-13E4 and AF 647-IgG1 have a similar MW (~156 kDa), thus sharing the same contribution of the paracellular transport in the overall permeability. The permeation rate of AF 647-MEM-189 was however much higher than of AF 647-13E4 and AF 647-IgG1 in "HBEC mono + HP + HA + HBEC" condition (Fig. 5C), confirming that MEM-189 was mainly transported by TfR-mediated transcytosis. Taken together, these results demonstrated our 3D BBB model with open structures could be useful for the study and the screening of molecules based on the TfR-mediated transport efficiency.

4. Conclusion

In this work, we successfully developed a 3D self-organized capillary network composed of endothelial cells, astrocytes and pericytes with perfusable opening ends. After 7 days culture, the obtained vascular network exhibited lumen which diameter was similar to the native BBB capillaries and also showed a few larger similar to microvessels and venules. Additionally, many BBB features could be retrieved in this model, including restricted paracellular transport, functional *P*-gp efflux system and specific transporters, such as the TfR. Since our 3D self-assembled BBB capillary network model was prepared in versatile commercial transwell, it can be easily used as a screening tool for toxicological and transport assays. The seeding density, cell ratios and gel volume could indeed be potentially tuned to match the dimensions of ≈6–96 microplates.

Immortalized cell lines of the three BBB cell types were preferred for the preparation of the model due their robustness and reproducibility, which are indeed desired by pharmaceutical companies for high-throughput screening assays. Nevertheless, ongoing work in the laboratory attempts to replace HBEC by human induced pluripotent stem cell-derived BMEC-like (hiPS-BMEC). HiPS-BMEC have attracted increasing attention in BBB modelling due to their ability to reproduce several BBB features, including physiologically relevant TEER, high expression of BMEC specific transporters and efflux pumps, and size-selective transport of molecules [13,63,64]. We recently reported hiPS-BMEC showed higher expression of some TJs and TfR, as well as a lower paracellular transport as compared to HBEC [42]. It could be interesting to know if hiPS-BMEC could form the same perfusable network with open structures than the one observed with HBEC in the fibrin gel.

Declaration of competing interest

The authors declare that they have no known competing financial interests or personal relationships that could have appeared to influence the work reported in this manuscript.

Acknowledgement

This work was supported by a Grant-in-Aid for Scientific Research (A) (20H00665), JST-COI NEXT (22-221035869), AMED-MPS (21be0304207h0005) and COCKPI-T funding of Takeda Pharmaceutical Company Limited.

Appendix A. Supplementary data

Supplementary data to this article can be found online at https://doi.org/10.1016/j.mtbio.2022.100324.

References

[1] N.J. Abbott, A.A.K. Patabendige, D.E.M. Dolman, S.R. Yusof, D.J. Begley, Structure and function of the blood–brain barrier, Neurobiol. Dis. 37 (2010) 13–25, https://doi.org/10.1016/j.nbd.2009.07.030.

[2] N.J. Abbott, Blood–brain barrier structure and function and the challenges for CNS drug delivery, J. Inherit. Metab. Dis. 36 (2013) 437–449, https://doi.org/10.1007/s10545-013-9608-0.

[3] J.M. Lajoie, E.V. Shusta, Targeting receptor-mediated transport for delivery of biologics across the blood-brain barrier, Annu. Rev. Pharmacol. Toxicol. 55 (2015) 613–631, https://doi.org/10.1146/annurev-pharmtox-010814-124852.

[4] W.M. Pardridge, J. Eisenberg, J. Yang, Human blood-brain barrier transferrin receptor, Metabolism 36 (1987) 892–895, https://doi.org/10.1016/0026-0495(87)90099-0.

[5] Z. Pang, H. Gao, Y. Yu, L. Guo, J. Chen, S. Pan, J. Ren, Z. Wen, X. Jiang, Enhanced intracellular delivery and chemotherapy for glioma rats by transferrin-conjugated biodegradable polymersomes loaded with doxorubicin, Bioconjugate Chem. 22 (2011) 1171–1180, https://doi.org/10.1021/bc200062q.

[6] R. Prades, S. Guerrero, E. Araya, C. Molina, E. Salas, E. Zurita, J. Selva, G. Egea, C. López-Iglesias, M. Teixidó, M.J. Kogan, E. Giralt, Delivery of gold nanoparticles to the brain by conjugation with a peptide that recognizes the transferrin receptor, Biomaterials 33 (2012) 7194–7205, https://doi.org/10.1016/j.biomaterials.2012.06.063.

[7] T. Kang, M. Jiang, D. Jiang, X. Feng, J. Yao, Q. Song, H. Chen, X. Gao, J. Chen, Enhancing glioblastoma-specific penetration by functionalization of nanoparticles with an iron-mimic peptide targeting transferrin/transferrin receptor complex, Mol. Pharm. 12 (2015) 2947–2961, https://doi.org/10.1021/acs.molpharmaceut.5b00222.

[8] S. Ruan, L. Qin, W. Xiao, C. Hu, Y. Zhou, R. Wang, X. Sun, W. Yu, Q. He, H. Gao, Acid-responsive transferrin dissociation and GLUT mediated exocytosis for increased blood–brain barrier transcytosis and programmed glioma targeting delivery, Adv. Funct. Mater. 28 (2018), 1802227, https://doi.org/10.1002/adfm.201802227.

[9] K. Hatherell, P.-O. Couraud, I.A. Romero, B. Weksler, G.J. Pilkington, Development of a three-dimensional, all-human in vitro model of the blood–brain barrier using mono-, co-, and tri-cultivation Transwell models, J. Neurosci. Methods 199 (2011) 223–229, https://doi.org/10.1016/j.jneumeth.2011.05.012.

[10] A. Appelt-Menzel, A. Cubukova, K. Günther, F. Edenhofer, J. Piontek, G. Krause, T. Stüber, H. Walles, W. Neuhaus, M. Metzger, Establishment of a human blood-brain barrier Co-culture model mimicking the neurovascular unit using induced pluri- and multipotent stem cells, Stem Cell Rep. 8 (2017) 894–906, https://doi.org/10.1016/j.stemcr.2017.02.021.

[11] N.L. Stone, T.J. England, S.E. O'Sullivan, A novel transwell blood brain barrier model using primary human cells, Front. Cell. Neurosci. 13 (2019), https://doi.org/10.3389/fncel.2019.00230.

[12] L. Cucullo, M. Hossain, V. Puvenna, N. Marchi, D. Janigro, The role of shear stress in Blood-Brain Barrier endothelial physiology, BMC Neurosci. 12 (2011) 40, https://doi.org/10.1186/1471-2202-12-40.

[13] G.D. Vatine, R. Barrile, M.J. Workman, S. Sances, B.K. Barriga, M. Rahnama, S. Barthakur, M. Kasendra, C. Lucchesi, J. Kerns, N. Wen, W.R. Spivia, Z. Chen, J. Van Eyk, C.N. Svendsen, Human iPSC-derived blood-brain barrier chips enable disease modeling and personalized medicine applications, Cell Stem Cell 24 (2019) 995–1005, https://doi.org/10.1016/j.stem.2019.05.011, e6.

[14] N.R. Wevers, D.G. Kasi, T. Gray, K.J. Wilschut, B. Smith, R. van Vught, F. Shimizu, Y. Sano, T. Kanda, G. Marsh, S.J. Trietsch, P. Vulto, H.L. Lanz, B. Obermeier, A perfused human blood–brain barrier on-a-chip for high-throughput assessment of barrier function and antibody transport, Fluids Barriers CNS 15 (2018) 23, https://doi.org/10.1186/s12987-018-0108-3.

[15] S.I. Ahn, Y.J. Sei, H.-J. Park, J. Kim, Y. Ryu, J.J. Choi, H.-J. Sung, T.J. MacDonald, A.I. Levey, Y. Kim, Microengineered human blood–brain barrier platform for understanding nanoparticle transport mechanisms, Nat. Commun. 11 (2020) 175, https://doi.org/10.1038/s41467-019-13896-7.

[16] S. Bang, S.-R. Lee, J. Ko, K. Son, D. Tahk, J. Ahn, C. Im, N.L. Jeon, A low permeability microfluidic blood-brain barrier platform with direct contact between perfusable vascular network and astrocytes, Sci. Rep. 7 (2017) 8083, https://doi.org/10.1038/s41598-017-07416-0.

[17] C. Kulczar, K.E. Lubin, S. Lefebvre, D.W. Miller, G.T. Knipp, Development of a direct contact astrocyte-human cerebral microvessel endothelial cells blood–brain barrier coculture model, J. Pharm. Pharmacol. 69 (2017) 1684–1696, https://doi.org/10.1111/jphp.12803.

[18] N.J. Abbott, L. Rönnbäck, E. Hansson, Astrocyte–endothelial interactions at the blood–brain barrier, Nat. Rev. Neurosci. 7 (2006) 41–53, https://doi.org/10.1038/nrn1824.

[19] M. Campisi, Y. Shin, T. Osaki, C. Hajal, V. Chiono, R.D. Kamm, 3D self-organized microvascular model of the human blood-brain barrier with endothelial cells, pericytes and astrocytes, Biomaterials 180 (2018) 117–129, https://doi.org/10.1016/j.biomaterials.2018.07.014.

[20] A. Herland, A.D. van der Meer, E.A. FitzGerald, T.-E. Park, J.J.F. Sleeboom, D.E. Ingber, Distinct contributions of astrocytes and pericytes to neuroinflammation identified in a 3D human blood-brain barrier on a chip, PLoS One 11 (2016), e0150360, https://doi.org/10.1371/journal.pone.0150360.

[21] H. Duvernoy, S. Delon, J.L. Vannson, The vascularization of the human cerebellar cortex, Brain Res. Bull. 11 (1983) 419–480, https://doi.org/10.1016/0361-9230(83)90116-8.

[22] S. Lee, M. Chung, S.-R. Lee, N.L. Jeon, 3D brain angiogenesis model to reconstitute functional human blood–brain barrier in vitro, Biotechnol. Bioeng. 117 (2020) 748–762, https://doi.org/10.1002/bit.27224.

[23] T.-E. Park, N. Mustafaoglu, A. Herland, R. Hasselkus, R. Mannix, E.A. FitzGerald, R. Prantil-Baun, A. Watters, O. Henry, M. Benz, H. Sanchez, H.J. McCrea, L.C. Goumnerova, H.W. Song, S.P. Palecek, E. Shusta, D.E. Ingber, Hypoxia-enhanced Blood-Brain Barrier Chip recapitulates human barrier function and shuttling of drugs and antibodies, Nat. Commun. 10 (2019) 2621, https://doi.org/10.1038/s41467-019-10588-0.

[24] A. Figarol, Y. Naka, Y. Shigemoto-Mogami, T. Furihata, K. Sato, M. Matsusaki, In Vitro self-organized three-dimensional model of the blood-brain barrier microvasculature, Biomed. Mater. 16 (2020), 015006, https://doi.org/10.1088/1748-605X/aba5f1.

[25] A. Figarol, M. Piantino, T. Furihata, T. Satoh, S. Sugiura, T. Kanamori, M. Matsusaki, Interstitial flow regulates in vitro three-dimensional self-organized brain micro-vessels, Biochem. Biophys. Res. Commun. 533 (2020) 600–606, https://doi.org/10.1016/j.bbrc.2020.09.061.

[26] D. Hikimoto, A. Nishiguchi, M. Matsusaki, M. Akashi, High-throughput blood- and lymph-capillaries with open-ended pores which allow the transport of drugs and cells, Advanced Healthcare Materials 5 (2016) 1969–1978, https://doi.org/10.1002/adhm.201600180.

[27] R. Ito, K. Umehara, S. Suzuki, K. Kitamura, K. Nunoya, Y. Yamaura, H. Imawaka, S. Izumi, N. Wakayama, T. Komori, N. Anzai, H. Akita, T. Furihata, A human immortalized cell-based blood–brain barrier triculture model: development and characterization as a promising tool for Drug−Brain permeability studies, Mol. Pharm. 16 (2019) 4461–4471, https://doi.org/10.1021/acs.molpharmaceut.9b00519.

[28] T. Furihata, R. Ito, A. Kamiichi, K. Saito, K. Chiba, Establishment and characterization of a new conditionally immortalized human astrocyte cell line, J. Neurochem. 136 (2016) 92–105, https://doi.org/10.1111/jnc.13358.

[29] K. Umehara, Y. Sun, S. Hiura, K. Hamada, M. Itoh, K. Kitamura, M. Oshima, A. Iwama, K. Saito, N. Anzai, K. Chiba, H. Akita, T. Furihata, A new conditionally immortalized human fetal brain pericyte cell line: establishment and functional characterization as a promising tool for human brain pericyte studies, Mol. Neurobiol. 55 (2018) 5993–6006, https://doi.org/10.1007/s12035-017-0815-9.

[30] D. Huang, E.A. Swanson, C.P. Lin, J.S. Schuman, W.G. Stinson, W. Chang, M.R. Hee, T. Flotte, K. Gregory, C.A. Puliafito, J.G. Fujimoto, Optical coherence tomography, Science 254 (1991) 1178–1181, https://doi.org/10.1126/science.1957169.

[31] B. Srinivasan, A.R. Kolli, M.B. Esch, H.E. Abaci, M.L. Shuler, J.J. Hickman, TEER measurement techniques for in vitro barrier model systems, J. Lab. Autom. 20 (2015) 107–126, https://doi.org/10.1177/2211068214561025.

[32] S. Nakagawa, M.A. Deli, H. Kawaguchi, T. Shimizudani, T. Shimono, Á. Kittel, K. Tanaka, M. Niwa, A new blood–brain barrier model using primary rat brain endothelial cells, pericytes and astrocytes, Neurochem. Int. 54 (2009) 253–263, https://doi.org/10.1016/j.neuint.2008.12.002.

[33] T. Kurosawa, Y. Tega, K. Higuchi, T. Yamaguchi, T. Nakakura, T. Mochizuki, H. Kusuhara, K. Kawabata, Y. Deguchi, Expression and functional characterization of drug transporters in brain microvascular endothelial cells derived from human induced pluripotent stem cells, Mol. Pharm. 15 (2018) 5546–5555, https://doi.org/10.1021/acs.molpharmaceut.8b00697.

[34] W.M. Pardridge, Blood-brain barrier biology and methodology, J. Neurovirol. 5 (1999) 556–569, https://doi.org/10.3109/13550289909021285.

[35] D. Shepro, N.M.L. Morel, Pericyte physiology, Faseb. J. 7 (1993) 1031–1038, https://doi.org/10.1096/fasebj.7.11.8370472.

[36] A. Nishiguchi, M. Matsusaki, M.R. Kano, H. Nishihara, D. Okano, Y. Asano, H. Shimoda, S. Kishimoto, S. Iwai, M. Akashi, In vitro 3D blood/lymph-vascularized human stromal tissues for preclinical assays of cancer metastasis, Biomaterials 179 (2018) 144–155, https://doi.org/10.1016/j.biomaterials.2018.06.019.

[37] R. Cabezas, M. Ávila, J. Gonzalez, R.S. El-Bachá, E. Báez, L.M. García-Segura, J.C. Jurado Coronel, F. Capani, G.P. Cardona-Gomez, G.E. Barreto, Astrocytic modulation of blood brain barrier: perspectives on Parkinson's disease, Front. Cell. Neurosci. 8 (2014) 211, https://doi.org/10.3389/fncel.2014.00211.

[38] A. Nishiguchi, M. Matsusaki, Y. Asano, H. Shimoda, M. Akashi, Effects of angiogenic factors and 3D-microenvironments on vascularization within sandwich cultures, Biomaterials 35 (2014) 4739–4748, https://doi.org/10.1016/j.biomaterials.2014.01.079.

[39] W.M. Pardridge, The blood-brain barrier: bottleneck in brain drug development, NeuroRx 2 (2005) 3–14, https://doi.org/10.1602/neurorx.2.1.3.

[40] A.M. Butt, H.C. Jones, N.J. Abbott, Electrical resistance across the blood-brain barrier in anaesthetized rats: a developmental study, J. Physiol. 429 (1990) 47–62, https://doi.org/10.1113/jphysiol.1990.sp018243.

[41] C. Crone, S.P. Olesen, Electrical resistance of brain microvascular endothelium, Brain Res. 241 (1982) 49–55, https://doi.org/10.1016/0006-8993(82)91227-6.

[42] M. Piantino, F. Louis, Y. Shigemoto-Mogami, K. Kitamura, K. Sato, T. Yamaguchi, K. Kawabata, S. Yamamoto, S. Iwasaki, H. Hirabayashi, M. Matsusaki, Brain microvascular endothelial cells derived from human induced pluripotent stem cells as in vitro model for assessing blood-brain barrier transferrin receptor-mediated transcytosis, Materials Today Bio 14 (2022), 100232, https://doi.org/10.1016/j.mtbio.2022.100232.

[43] A.S. Easton, M.H. Sarker, P.A. Fraser, Two components of blood-brain barrier disruption in the rat, J. Physiol. 503 (1997) 613–623, https://doi.org/10.1111/j.1469-7793.1997.613bg.x.

[44] A. Drolez, E. Vandenhaute, S. Julien, F. Gosselet, J. Burchell, R. Cecchelli, P. Delannoy, M.-P. Dehouck, C. Mysiorek, Selection of a relevant in vitro blood-brain barrier model to investigate pro-metastatic features of human breast cancer cell lines, PLoS One 11 (2016), e0151155, https://doi.org/10.1371/journal.pone.0151155.

[45] Y. Molino, F. Jabès, E. Lacassagne, N. Gaudin, M. Khrestchatisky, Video Article Setting-Up an In Vitro Model of Rat Blood-brain Barrier (BBB): A Focus on BBB Impermeability and Receptor-Mediated Transport, 2014.

[46] W. Yuan, Y. Lv, M. Zeng, B.M. Fu, Non-invasive measurement of solute permeability in cerebral microvessels of the rat, Microvasc. Res. 77 (2009) 166–173, https://doi.org/10.1016/j.mvr.2008.08.004.

[47] A. Reichel, D.J. Begley, N.J. Abbott, An overview of in vitro techniques for blood-brain barrier studies, in: S. Nag (Ed.), The Blood-Brain Barrier: Biology and Research Protocols, Humana Press, Totowa, NJ, 2003, pp. 307–324, https://doi.org/10.1385/1-59259-419-0:307.

[48] K.J. Hewitt, R. Agarwal, P.J. Morin, The claudin gene family: expression in normal and neoplastic tissues, BMC Cancer 6 (2006) 186, https://doi.org/10.1186/1471-2407-6-186.

[49] A.S. Fanning, B.J. Jameson, L.A. Jesaitis, J.M. Anderson, The tight junction protein ZO-1 establishes a link between the transmembrane protein occludin and the actin cytoskeleton, J. Biol. Chem. 273 (1998) 29745–29753, https://doi.org/10.1074/jbc.273.45.29745.

[50] K. Umeda, J. Ikenouchi, S. Katahira-Tayama, K. Furuse, H. Sasaki, M. Nakayama, T. Matsui, S. Tsukita, M. Furuse, S. Tsukita, ZO-1 and ZO-2 independently determine where claudins are polymerized in tight-junction strand formation, Cell 126 (2006) 741–754, https://doi.org/10.1016/j.cell.2006.06.043.

[51] C.M. Van Itallie, A.S. Fanning, J. Holmes, J.M. Anderson, Occludin is required for cytokine-induced regulation of tight junction barriers, J. Cell Sci. 123 (2010) 2844–2852, https://doi.org/10.1242/jcs.065581.

[52] S. Seetharaman, M.A. Barrand, L. Maskell, R.J. Scheper, Multidrug resistance-related transport proteins in isolated human brain microvessels and in cells cultured from these isolates, J. Neurochem. 70 (1998) 1151–1159, https://doi.org/10.1046/j.1471-4159.1998.70031151.x.

[53] S. Dauchy, F. Dutheil, R.J. Weaver, F. Chassoux, C. Daumas-Duport, P.-O. Couraud, J.-M. Scherrmann, I. De Waziers, X. Declèves, ABC transporters, cytochromes P450 and their main transcription factors: expression at the human blood–brain barrier, J. Neurochem. 107 (2008) 1518–1528, https://doi.org/10.1111/j.1471-4159.2008.05720.x.

[54] L. Lescale-Matys, J. Dyer, D. Scott, T.C. Freeman, E.M. Wright, S.P. Shirazi-Beechey, Regulation of the ovine intestinal Na+/glucose co-transporter (SGLT1) is dissociated from mRNA abundance, Biochem. J. 291 (1993) 435–440, https://doi.org/10.1042/bj2910435.

[55] M. Fontaine, W.F. Elmquist, D.W. Miller, Use of rhodamine 123 to examine the functional activity of P-glycoprotein in primary cultured brain microvessel endothelial cell monolayers, Life Sci. 59 (1996) 1521–1531, https://doi.org/10.1016/0024-3205(96)00483-3.

[56] W. Löscher, H. Potschka, Blood-brain barrier active efflux transporters: ATP-binding cassette gene family, NeuroRx 2 (2005) 86–98, https://doi.org/10.1602/neurorx.2.1.86.

[57] H. Sun, H. Dai, N. Shaik, W.F. Elmquist, Drug efflux transporters in the CNS, Adv. Drug Deliv. Rev. 55 (2003) 83–105, https://doi.org/10.1016/S0169-409X(02)00172-2.

[58] J.B. Fishman, J.B. Rubin, J.V. Handrahan, J.R. Connor, R.E. Fine, Receptor-mediated transcytosis of transferrin across the blood-brain barrier, J. Neurosci. Res. 18 (1987) 299–304, https://doi.org/10.1002/jnr.490180206.

[59] A. Calzolari, L.M. Larocca, S. Deaglio, V. Finisguerra, A. Boe, C. Raggi, L. Ricci-Vitani, F. Pierconti, F. Malavasi, R. De Maria, U. Testa, R. Pallini, Transferrin receptor 2 is frequently and highly expressed in glioblastomas, Transl Oncol 3 (2010) 123–134, https://doi.org/10.1593/tlo.09274.

[60] Z.M. Qian, H. Li, H. Sun, K. Ho, Targeted drug delivery via the transferrin receptor-mediated endocytosis pathway, Pharmacol. Rev. 54 (2002) 561–587, https://doi.org/10.1124/pr.54.4.561.

[61] K.B. Johnsen, A. Burkhart, L.B. Thomsen, T.L. Andresen, T. Moos, Targeting the transferrin receptor for brain drug delivery, Prog. Neurobiol. 181 (2019), 101665, https://doi.org/10.1016/j.pneurobio.2019.101665.

[62] H. Sade, C. Baumgartner, A. Hugenmatter, E. Moessner, P.-O. Freskgård, J. Niewoehner, A human blood-brain barrier transcytosis assay reveals antibody transcytosis influenced by pH-dependent receptor binding, PLoS One 9 (2014), e96340, https://doi.org/10.1371/journal.pone.0096340.

[63] E.S. Lippmann, S.M. Azarin, J.E. Kay, R.A. Nessler, H.K. Wilson, A. Al-Ahmad, S.P. Palecek, E.V. Shusta, Human blood-brain barrier endothelial cells derived from pluripotent stem cells, Nat. Biotechnol. 30 (2012) 783–791, https://doi.org/10.1038/nbt.2247.

[64] E.S. Lippmann, A. Al-Ahmad, S.M. Azarin, S.P. Palecek, E.V. Shusta, A retinoic acid-enhanced, multicellular human blood-brain barrier model derived from stem cell sources, Sci. Rep. 4 (2014) 4160, https://doi.org/10.1038/srep04160.